



Strong electronic correlations in interstitial magnetic centers of zero-dimensional electride β -Yb₅Sb₃Dmitry Y. Novoselov ^{1,2,3,*} Vladimir I. Anisimov,^{1,2,3} and Artem R. Oganov ³¹*M. N. Mikheev Institute of Metal Physics of Ural Branch of Russian Academy of Sciences, 18 S. Kovalevskaya St., Yekaterinburg 620137, Russia*²*Department of Theoretical Physics and Applied Mathematics, Ural Federal University, 19 Mira St., Yekaterinburg 620002, Russia*³*Skolkovo Institute of Science and Technology, 3 Nobel St., Moscow 143026, Russia*

(Received 13 April 2021; accepted 21 May 2021; published 14 June 2021)

Using dynamical mean-field theory, we investigate the correlated nature of quantum-confined electrons localized in the crystal voids of the zero-dimensional electride β -Yb₅Sb₃. In this work, maximally localized Wannier functions were used to obtain an analytical description of the half-filled electride electronic states and to establish a high degree of their localization, with the magnetic moment of $1\mu_B$ per anionic cavity. We reproduced the Mott metal-insulator transition, obtained the experimentally observed energy gap, and demonstrated the decrease of resistivity with increasing temperature, typical for semiconductors. The Curie-type temperature dependence of the compound's magnetic susceptibility was calculated and found to be in close agreement with experiment. These results obtained prove that the Coulomb correlations between the localized anionic electrons are the source of the observed electronic and magnetic properties of β -Yb₅Sb₃.

DOI: [10.1103/PhysRevB.103.235126](https://doi.org/10.1103/PhysRevB.103.235126)**I. INTRODUCTION**

Since their discovery [1,2], electrides have attracted the increasing attention of researchers due to their exotic state of quantum-confined electrons located in the periodic crystal voids and not associated with the atoms of the crystal structure [3–7]. Quantum confinement occurs when an electron or a hole falls into a potential well whose width is comparable to the electron wavelength. Electrons in electrides are the simplest anions. On the other hand, because of their small mass and related quantum effects, the captured electrons can participate in more complex interactions with each other and with cations. As a result, electrides can exhibit sophisticated and diverse properties, providing a rich field for experiments and theoretical research. The low-dimensional topology of the cavities and partial occupation of the electride states can cause correlations between the trapped electrons, leading to intriguing properties of such systems. For example, it has been shown that correlation effects occurring in the electride states in elemental calcium cause the formation of a simple cubic structure under pressure [8,9]. Strong interstitial electronic localization is responsible for the metal-semiconductor transition in lithium [10,11] and the insulating state of Na₂He [12] under pressure, and makes the high-pressure electride phase of sodium optically transparent [13]. For low-dimensional electrides, such as the layered two-dimensional (2D) electrides Ca₂N [14,15], Y₂C [16], and Gd₂C [17], the existence of Stoner-type magnetism [5] has been predicted.

In all the cases we know, electrides have an excess of cations and usually contain atoms of highly electropositive elements (such as alkali metals, alkaline-earth metals,

and rare-earth metals), from which electrons can be easily removed and put into the interstitial space. The low dimensionality of the cavities leads to a more pronounced localization of the electride states. Dimorphic Yb₅Sb₃ can crystallize in α - or β -Yb₅Sb₃ phases with the hexagonal $P6_3/mcm$ or orthorhombic $Pnma$ structure, respectively [18,19]. According to the latest scale of electronegativity [20], Yb has the lowest electronegativity among lanthanoids, and one of the lowest (or possibly the lowest) among all elements. Both phases of Yb₅Sb₃ contain ytterbium atoms in the oxidation state 2+ and one excess electron per formula unit (f.u.), so the formula can be written as [Yb₅Sb₃]⁺ · e⁻. In the α phase, the interstitial space is quasi-one-dimensional, formed by the chains of Yb₆ octahedra running along the c axis. β -Yb₅Sb₃ contains anionic electrons confined within the Yb₄ tetrahedra and is a zero dimensional (0D) electride. Since in the 0D case the charge density is more localized than in the one-dimensional (1D) case, the corresponding electride energy states are described by flatter bands [19]. This means that the electronic correlation effects should manifest themselves most clearly in β -Yb₅Sb₃.

Despite these interstitial states being partially filled, β -Yb₅Sb₃ shows a semiconducting behavior and Curie-type temperature dependence of the magnetic susceptibility [19]. Besides, Lu *et al.* [19] argue that β -Yb₅Sb₃ may be treated as a strongly correlated material, and electronic correlations between the anionic electrons play an important role in its physics. But standard approximations of density functional theory (DFT) fail to describe the band structure and the paramagnetic phase of β -Yb₅Sb₃ [19]. It is interesting to evaluate the strength and realize the role of Coulomb correlations between the 0D-cavity-trapped electrons in forming the observed electronic and magnetic properties of β -Yb₅Sb₃.

*novoselov@imp.uran.ru

In this work, we investigate the mechanism underlying the metal-insulator transition and semiconducting behavior, estimate the degree of localization of the electrone electrons in the lattice interstices and the strength of the electron-electron Coulomb interaction, and analyze the response of the system to an external magnetic field. Neither DFT nor DFT+ U methods can properly reproduce the band and magnetic structure of β -Yb₅Sb₃ [19]. Therefore, we use maximally localized Wannier functions (MLWFs) to describe the anionic electronic states and the approach combining the DFT with the dynamical mean-field theory (DFT+DMFT) as the main tool for modeling the correlated electronic structure to study the role of anionic electrons in determining the electronic and magnetic properties of β -Yb₅Sb₃.

II. METHODS

To obtain the noninteracting band structure $\varepsilon(\vec{k})$, DFT calculations were carried out with the pseudopotentials supplied with the QUANTUM ESPRESSO package [21] using the Perdew-Burke-Ernzerhof exchange-correlation functional [22]. The initial structural data for β -Yb₅Sb₃ were taken from Ref. [23]. Integration in reciprocal space was done on a regular $6 \times 5 \times 4$ k -point mesh in the irreducible part of the Brillouin zone. The energy cutoff for plane-wave wave functions and charge-density expansion has been set to 60 Ry and 480 Ry, respectively. The MLWF basis was obtained by using the WANNIER90 package [24], which was also used to extract the noninteracting generalized gradient approximation (GGA) Hamiltonian H_{GGA} in real space. The DFT+DMFT approach [25,26] was used to take into account the Coulomb correlations and many-body effects for the constructed Hamiltonian. The DFT+DMFT calculations were performed for the inverse temperature values $\beta = 1/k_B T$ from 5 to 90 eV⁻¹, where k_B is the Boltzmann constant and T is the absolute temperature. A simplified fully-localized-limit form was used for the double-counting correction during the self-consistent DMFT loop. The effective DMFT quantum impurity problem [27] was solved using the continuous-time quantum Monte Carlo method with the hybridization expansion algorithm [28] from the AMULET package [29]. The analytical continuation of the self-energy dependence to the real frequencies was evaluated by using the Padé approximation method [30].

III. RESULTS AND DISCUSSION

A. Interstitial electronic states

In β -Yb₅Sb₃, the states of the anionic electrons localized in the periodic 0D spaces inside Yb₄ tetrahedra correspond to the energy bands crossing the Fermi level and are well separated from the bands of the nearest ions. To describe these electrone electronic states, we constructed four MLWFs projected within the energy window spanned by four energy bands crossing the Fermi level (Fig. 1) and centered in the tetrahedral voids [Figs. 2(b)–2(d)] [24,31–35]. The obtained MLWFs represent the electrone states [15] and predominantly have the symmetry of an s orbital. The contribution of the MLWFs to the band structure is shown in Fig. 1.

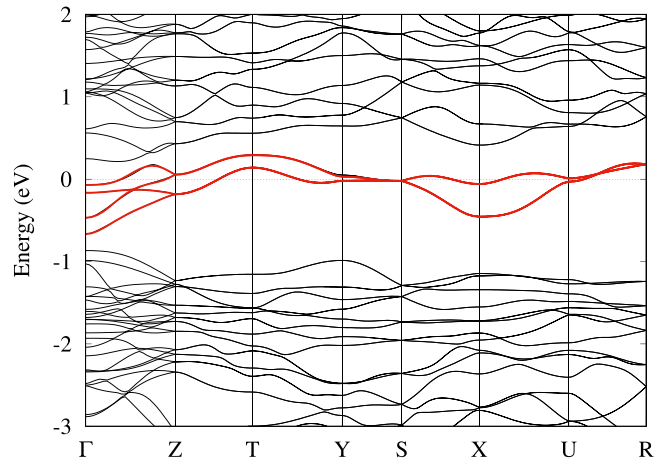


FIG. 1. Band structure of β -Yb₅Sb₃ (black lines). The contribution to the Bloch states by the maximally localized Wannier function centered on the tetrahedral interstitial voids is located in the energy window from -0.8 to 0.3 eV and is shown in red.

The electrone Wannier functions also effectively contain the contributions from the states of Yb atoms forming the tetrahedron and an essential part from the states of the nearest Sb atoms located between the tetrahedra [yellow and blue areas of the isosurface in Figs. 2(b)–2(d)]. These contributions are due to the hybridization between the electrone and the $5p$ states of antimony and provide an indirect interaction channel

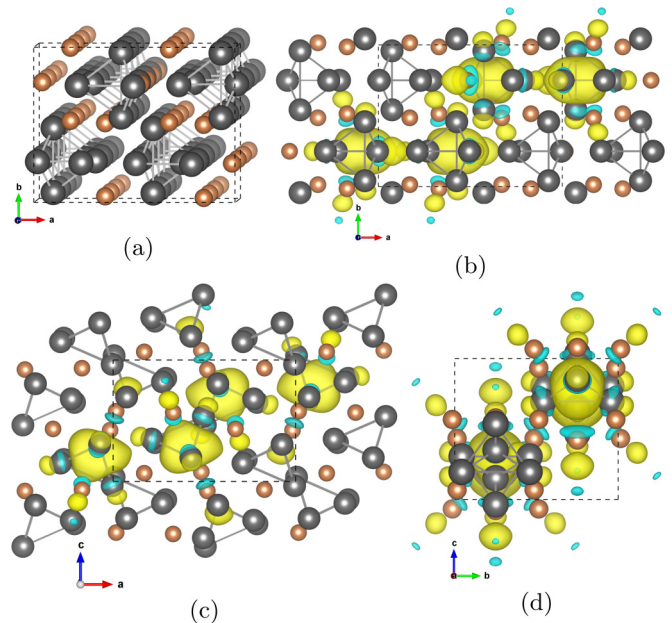


FIG. 2. Crystal structure of (a) β -Yb₅Sb₃ and isosurface of the spatial distribution of the MLWFs describing the electrone state in the (ab) , (ac) , and (bc) planes in panels (b)–(d), respectively. Panel (d) shows only the atoms making the main contribution to the obtained MLWFs. The yellow and blue colors of the isosurface correspond to the positive and negative parts of the wave function, respectively. The Yb and Sb atoms are shown in dark gray and orange, respectively. Dashed line contours denote the unit-cell boundary.

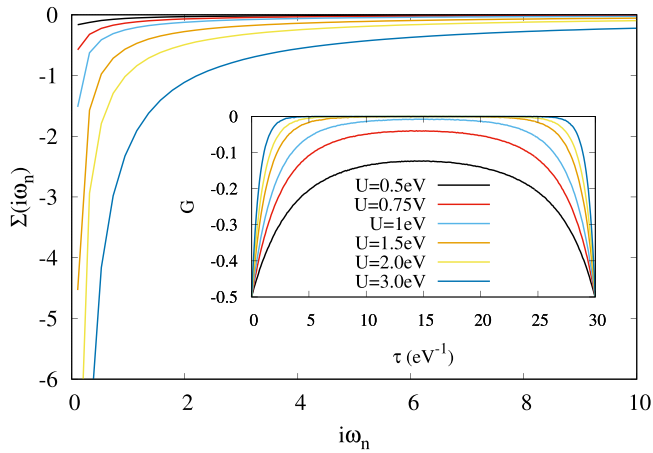


FIG. 3. Imaginary part of the self-energy as a function of the Matsubara frequencies at $\beta = 30 \text{ eV}^{-1}$ for different values of the Coulomb parameter U . The corresponding Green's functions for one impurity are shown in the inset.

between the electrons localized in the cavities of the neighboring tetrahedra. The obtained Wannier functions were used as a basis to construct the noninteracting Hamiltonian.

B. Mott metal-insulator transition

The resulting Hamiltonian was solved using DMFT [25,26,29]. To study the metal-insulator transition, DMFT calculations were performed for several values of the Coulomb parameter U in the range 0.5 to 3 eV. The dependencies of the self-energy on Matsubara frequencies and of the Green's

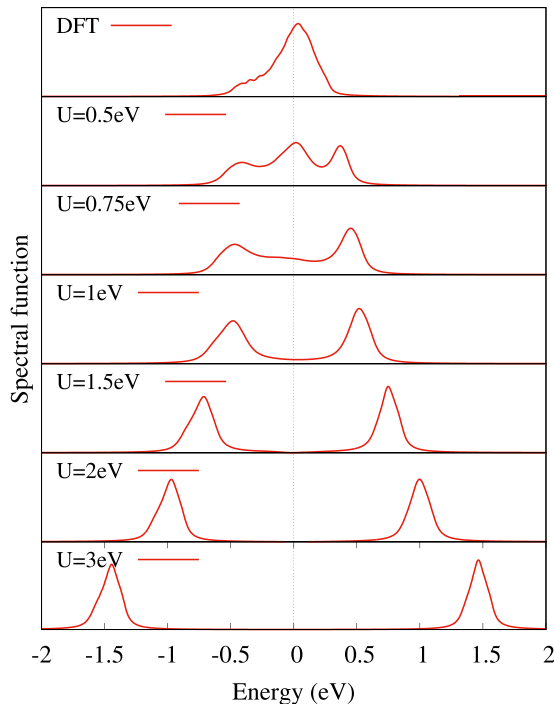


FIG. 4. Spectral functions obtained using the DFT (top panel) and the DFT+DMFT for different values of U at $\beta = 30 \text{ eV}^{-1}$. Zero corresponds to Fermi energy.

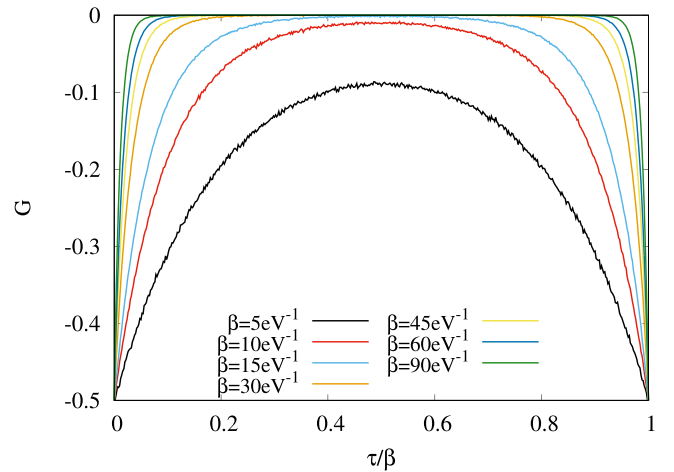


FIG. 5. Green's functions at $U = 2 \text{ eV}$ for different values of β parameter.

functions on the imaginary time, obtained in the DMFT calculations, are shown in Fig. 3 for one impurity. For all other impurities, similar behavior was observed. The value of Green's function at $\tau = \beta/2 \text{ eV}^{-1}$ indicates the evolution from a metal to an insulator, with the increasing U , via a semimetallic state caused by a split of the half-filled degenerate electrone bands into a filled and an empty one. All the self-energy functions diverge at zero, indicating a sharp increase in the localization of the electronic states at the tetrahedral voids as U rises (Fig. 3).

To analyze the evolution of the electrone bands during the metal-insulator transition, spectral functions were evaluated using an analytical continuation of the self-energy dependence to the real frequencies (Fig. 4). In the absence of electronic correlations, the electrone states form a peak at the Fermi level (Fig. 4, top panel). At a small value of $U = 0.5 \text{ eV}$, a three-peak structure begins to form, with a central quasi-particle peak and upper and lower Hubbard bands which are typical for moderate correlations. As U rises to 0.75 eV, the quasiparticle peak at the Fermi level disappears and the Hubbard bands become well pronounced. Further growth of the Coulomb parameter to 1.5 eV is accompanied by the formation of the semimetallic state with a gradual decrease in the density of states at the Fermi level. At $U \geq 1.5 \text{ eV}$, the energy gap gradually opens and a transition to the strongly correlated Mott insulator state occurs. At $U = 2 \text{ eV}$, the energy gap is about 0.5 eV, which is close to the experimental estimates [19]. This demonstrates that the Mott insulator state in $\beta\text{-Yb}_5\text{Sb}_3$ electrone exists because of the Coulomb interactions of the electrons not related to specific atom sites of the crystal structure.

Varying the β value, while the Coulomb parameter was fixed at $U = 2 \text{ eV}$, we obtained the set of the Green's functions shown in Fig. 5 for one impurity (for other impurities, the results are qualitatively indistinguishable). A decrease in temperature leads to an enhancement of the insulator nature of Green's functions, which is typical for semiconductors. This observation agrees with experiment [19], which means that the semiconducting behavior of $\beta\text{-Yb}_5\text{Sb}_3$ is caused by Coulomb correlations between the electrone electrons.

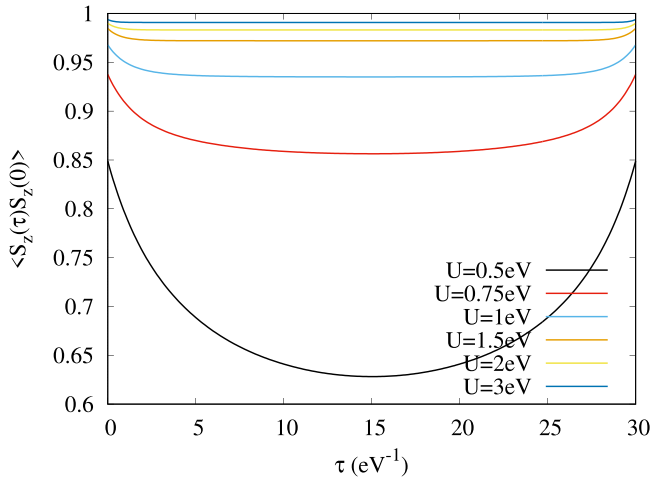


FIG. 6. Local spin-spin correlation functions $\langle S_z(\tau)S_z(0) \rangle$ in the imaginary-time domain obtained using the DFT+DMFT method at $\beta = 30 \text{ eV}^{-1}$ for different values of the Coulomb parameter U .

C. Localization and magnetism

We studied the magnetic properties of the electrider states of $\beta\text{-Yb}_5\text{Sb}_3$, starting with the analysis of the lifetime of local moments by evaluating the behavior of the local spin-spin correlation function $\langle S_z(\tau)S_z(0) \rangle$ on the imaginary-time axis. The less the correlator depends on the imaginary time, the more localized the magnetic moments become. For strongly localized magnetic moments, the correlator is constant, $\langle S_z(\tau)S_z(0) \rangle \approx S^2$, which is typical for highly correlated systems. Such a behavior was observed already for $U \geq 1.5 \text{ eV}$ (Fig. 6). At $U = 2 \text{ eV}$, each of anionic electrons acts as a magnetic center with a highly localized magnetic moment with the root of the instant squared magnetic moment $(\langle m_z^2 \rangle)^{1/2} \approx 0.99 \mu_B$ corresponding to one electron with the spin $S = 1/2$ accommodated in the tetrahedral interstice.

To analyze the contribution of the electrider subsystem to the magnetic response to an external magnetic field, we calculated the temperature dependence of the uniform magnetic susceptibility $\chi(T) = m(T)/H_z$, where $m(T) = \sum_m (n_m^\uparrow - n_m^\downarrow)$ is the magnetization. For this purpose, DMFT calculations were performed for the inverse temperature β in the range from 10 to 90 eV^{-1} . The $\chi(T)$ dependence (Fig. 7) was obtained using DMFT for different values of U from 0.5 to 5 eV by applying a small external magnetic field to the Hamiltonian and measuring the magnetization [15].

In the paramagnetic phase, for all the values of the Coulomb parameter U , the uniform susceptibility strictly follows the Curie-Weiss law. In the temperature range considered, the dependence of the uniform magnetic susceptibility agrees best with experiment at $U = 2 \text{ eV}$ [19]. This value of the U parameter is reasonable for s -electron systems [35,36] but is small in comparison with the U values for d -electron systems [32,33,37–43]. At the same time, the strength of the electronic correlations is determined rather by the U/W ratio, where W is bandwidth, and for $\beta\text{-Yb}_5\text{Sb}_3$ it is estimated as $U/W > 1$ due to very narrow bands, which is typical for strongly correlated materials such as transition-metal oxides, rare earths, Kondo systems, etc.

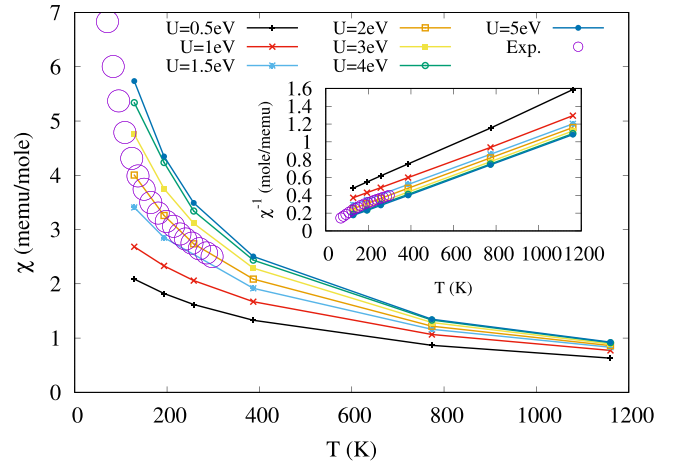


FIG. 7. Temperature dependencies of the uniform magnetic susceptibility $\chi(T)$ and its inverse (in the inset) for different values of U . The experimental data [19] are shown by purple circles.

The Weiss constant Θ estimated from the extrapolated χ^{-1} is negative for all values considered of the Coulomb parameter U , indicating the presence of antiferromagnetic (AFM) fluctuations, which is consistent with the assumption of Lu *et al.* [19] about the presence of AFM components in the magnetic interaction between anionic electrons. The AFM interaction has a superexchange nature and occurs via the $5p$ orbitals of the antimony atoms located on the faces of neighboring Yb_4 tetrahedra. Thus the model mainly derived from the interstitial anionic electronic states properly describes the magnetic features of $\beta\text{-Yb}_5\text{Sb}_3$ with the moderate value of the Coulomb parameter U .

IV. CONCLUSIONS

By applying the DFT+DMFT approach to $\beta\text{-Yb}_5\text{Sb}_3$ compound, we showed that the electrons described by the half-filled electrider wave functions centered in the tetrahedral voids are highly localized and have large magnetic moments of $\approx 1\mu_B$. The model that includes only the electrider states is capable of reproducing the Mott metal-insulator transition with increasing the Coulomb parameter U , the experimentally observed insulating state, and the semiconducting behavior with temperature. We also established that it is the electrider subsystem that leads to the existence of the experimentally observed Curie-Weiss temperature dependence of the magnetic susceptibility, which indicates the tendency to an indirect magnetic interaction between the interstitial magnetic centers via the $5p$ states of the Sb atoms located between the nearest Yb_4 tetrahedra. This proves that the phenomena described are caused by the strong Coulomb correlations between the electrider electrons.

ACKNOWLEDGMENTS

The DFT and MLWF parts of the study were supported by the Ministry of Science and Higher Education of the Russian Federation (No. AAAA-A18-118020190098-5, topic “Electron”). DMFT calculations were carried out within the state assignment of the Russian Science Foundation (Project 19-72-30043).

- [1] J. L. Dye, Chemistry: Electrons as anions, *Science* **301**, 607 (2003).
- [2] J. L. Dye, Electrides: Early examples of quantum confinement, *Acc. Chem. Res.* **42**, 1564 (2009).
- [3] M. Hirayama, S. Matsuishi, H. Hosono, and S. Murakami, Electrides As A New Platform Of Topological Materials, *Phys. Rev. X* **8**, 031067 (2018).
- [4] C. Park, S. W. Kim, and M. Yoon, First-Principles Prediction of New Electrides with Nontrivial Band Topology Based on One-Dimensional Building Blocks, *Phys. Rev. Lett.* **120**, 026401 (2018).
- [5] X. Sui, J. Wang, and W. Duan, Prediction of stoner-type magnetism in low-dimensional electrides, *J. Phys. Chem. C* **123**, 5003 (2019).
- [6] C. Liu, S. A. Nikolaev, W. Ren, and L. A. Burton, Electrides: A review, *J. Mater. Chem. C* **8**, 10551 (2020).
- [7] H. Hosono and M. Kitano, Advances in materials and applications of inorganic electrides, *Chem. Rev.* **121**, 3121 (2021).
- [8] D. Y. Novoselov, D. M. Korotin, A. O. Shorikov, A. R. Oganov, and V. I. Anisimov, Interplay between the Coulomb interaction and hybridization in Ca and anomalous pressure dependence of the resistivity, *JETP Lett.* **109**, 387 (2019).
- [9] D. Y. Novoselov, D. M. Korotin, A. O. Shorikov, A. R. Oganov, and V. I. Anisimov, Weak Coulomb correlations stabilize the electride high-pressure phase of elemental calcium, *J. Phys.: Condens. Matter* **32**, 445501 (2020).
- [10] Y. Ma, A. R. Oganov, and Y. Xie, High-pressure structures of lithium, potassium, and rubidium predicted by an *ab initio* evolutionary algorithm, *Phys. Rev. B* **78**, 014102 (2008).
- [11] T. Matsuoka and K. Shimizu, Direct observation of a pressure-induced metal-to-semiconductor transition in lithium, *Nature (London)* **458**, 186 (2009).
- [12] X. Dong, A. R. Oganov, A. F. Goncharov, E. Stavrou, S. Lobanov, G. Saleh, G.-R. Qian, Q. Zhu, C. Gatti, V. L. Deringer, R. Dronskowski, X.-F. Zhou, V. B. Prakapenka, Z. Konôpková, I. A. Popov, A. I. Boldyrev, and H.-T. Wang, A stable compound of helium and sodium at high pressure, *Nat. Chem.* **9**, 440 (2017).
- [13] Y. Ma, M. Eremets, A. R. Oganov, Y. Xie, I. Trojan, S. Medvedev, A. O. Lyakhov, M. Valle, and V. Prakapenka, Transparent dense sodium, *Nature (London)* **458**, 182 (2009).
- [14] J. S. Oh, C. J. Kang, Y. J. Kim, S. Sinn, M. Han, Y. J. Chang, B. G. Park, S. W. Kim, B. I. Min, H. D. Kim, and T. W. Noh, Evidence for anionic excess electrons in a quasi-two-dimensional Ca_2N electride by angle-resolved photoemission spectroscopy, *J. Am. Chem. Soc.* **138**, 2496 (2016).
- [15] D. Y. Novoselov, D. M. Korotin, A. O. Shorikov, V. I. Anisimov, and A. R. Oganov, Interacting electrons in 2D-electride Ca_2N , *J. Phys. Chem. C* (to be published).
- [16] M. Hiraishi, K. M. Kojima, I. Yamauchi, H. Okabe, S. Takeshita, A. Koda, R. Kadono, X. Zhang, S. Matsuishi, H. Hosono, K. Hirata, S. Otani, and N. Ohashi, Electronic correlation in the quasi-two-dimensional electride Y_2C , *Phys. Rev. B* **98**, 041104(R) (2018).
- [17] S. Y. Lee, J.-Y. Hwang, J. Park, C. N. Nandadasa, Y. Kim, J. Bang, K. Lee, K. H. Lee, Y. Zhang, Y. Ma, H. Hosono, Y. H. Lee, S.-G. Kim, and S. W. Kim, Ferromagnetic quasi-atomic electrons in two-dimensional electride, *Nat. Commun.* **11**, 1526 (2020).
- [18] G. D. Brunton and H. Steinfink, Crystal structure of β -ytterbium triantimonide, a low-temperature phase, *Inorg. Chem.* **10**, 2301 (1971).
- [19] Y. Lu, J. Wang, J. Li, J. Wu, S. Kanno, T. Tada, and H. Hosono, Realization of Mott-insulating electrides in dimorphic YB_5Sb_3 , *Phys. Rev. B* **98**, 125128 (2018).
- [20] C. Tantardini and A. R. Oganov, Thermochemical electronegativities of the elements, *Nat. Commun.* **12**, 2087 (2021).
- [21] P. Giannozzi, S. Baroni, N. Bonini, M. Calandra, R. Car, C. Cavazzoni, D. Ceresoli, G. L. Chiarotti, M. Cococcioni, I. Dabo, A. Dal Corso, S. de Gironcoli, S. Fabris, G. Fratesi, R. Gebauer, U. Gerstmann, C. Gougoussis, A. Kokalj, M. Lazzeri, L. Martin-Samos, N. Marzari, F. Mauri, R. Mazzarello, S. Paolini, A. Pasquarello, L. Paulatto, C. Sbraccia, S. Scandolo, G. Sclauzero, A. P. Seitsonen, A. Smogunov, P. Umari, and R. M. Wentzcovitch, QUANTUM ESPRESSO: A modular and open-source software project for quantum simulations of materials, *J. Phys.: Condens. Matter* **21**, 395502 (2009).
- [22] J. P. Perdew, K. Burke, and M. Ernzerhof, Generalized Gradient Approximation Made Simple, *Phys. Rev. Lett.* **77**, 3865 (1996).
- [23] E. Leon-Escamilla and J. D. Corbett, Hydrogen stabilization, *J. Alloys Compd.* **265**, 104 (1998).
- [24] A. A. Mostofi, J. R. Yates, G. Pizzi, Y.-S. Lee, I. Souza, D. Vanderbilt, and N. Marzari, An updated version of Wannier90: A tool for obtaining maximally-localised Wannier functions, *Comput. Phys. Commun.* **185**, 2309 (2014).
- [25] V. I. Anisimov, A. I. Poteryaev, M. A. Korotin, A. O. Anokhin, and G. Kotliar, First-principles calculations of the electronic structure and spectra of strongly correlated systems: Dynamical mean-field theory, *J. Phys.: Condens. Matter* **9**, 7359 (1997).
- [26] K. Held, I. A. Nekrasov, G. Keller, V. Eyert, N. Blümer, A. K. McMahan, R. T. Scalettar, T. Pruschke, V. I. Anisimov, and D. Vollhardt, Realistic investigations of correlated electron systems with LDA+DMFT, *Phys. Status Solidi B* **243**, 2599 (2006).
- [27] P. Werner and A. J. Millis, Hybridization expansion impurity solver: General formulation and application to Kondo lattice and two-orbital models, *Phys. Rev. B* **74**, 155107 (2006).
- [28] E. Gull, A. J. Millis, A. I. Lichtenstein, A. N. Rubtsov, M. Troyer, and P. Werner, Continuous-time Monte Carlo methods for quantum impurity models, *Rev. Mod. Phys.* **83**, 349 (2011).
- [29] <http://www.amulet-code.org>.
- [30] H. J. Vidberg and J. W. Serene, Solving the Eliashberg equations by means of N -point Padé approximants, *J. Low Temp. Phys.* **29**, 179 (1977).
- [31] N. Marzari and D. Vanderbilt, Maximally localized generalized Wannier functions for composite energy bands, *Phys. Rev. B* **56**, 12847 (1997).
- [32] D. Y. Novoselov, D. M. Korotin, A. O. Shorikov, and V. I. Anisimov, Charge and spin degrees of freedom in strongly correlated systems: Mott states opposite Hund's metals, *J. Phys.: Condens. Matter* **32**, 235601 (2020).
- [33] D. Novoselov, D. M. Korotin, and V. I. Anisimov, Spin state transition in the active center of the hemoglobin molecule: DFT+DMFT study, *JETP Lett.* **103**, 658 (2016).
- [34] D. Novoselov, D. M. Korotin, and V. I. Anisimov, Hellmann-Feynman forces within the DFT+ U in Wannier functions basis, *J. Phys.: Condens. Matter* **27**, 325602 (2015).

- [35] D. M. Korotin, D. Novoselov, and V. I. Anisimov, Correlation effects and phonon modes softening with doping in $\text{Ba}_{1-x}\text{K}_x\text{BiO}_3$, *J. Phys.: Condens. Matter* **26**, 195602 (2014).
- [36] D. Korotin, V. Kukolev, A. V. Kozhevnikov, D. Novoselov, and V. I. Anisimov, Electronic correlations and crystal structure distortions in BaBiO_3 , *J. Phys.: Condens. Matter* **24**, 415603 (2012).
- [37] Y.-C. Wang and H. Jiang, Local screened Coulomb correction approach to strongly correlated d -electron systems, *J. Chem. Phys.* **150**, 154116 (2019).
- [38] D. M. Korotin, D. Novoselov, and V. I. Anisimov, Parao-orbital ground state of the trivalent Ni ion in LiNiO_2 from DFT+DMFT calculations, *Phys. Rev. B* **99**, 045106 (2019).
- [39] D. Novoselov, D. M. Korotin, and V. I. Anisimov, Correlations induced orbital ordering and cooperative Jahn–Teller distortion in the paramagnetic insulator KCrF_3 , *JETP Lett.* **103**, 573 (2016).
- [40] Y. S. Ponosov and D. Y. Novoselov, Lattice and spin excitations of YFeO_3 : A Raman and density functional theory study, *Phys. Rev. B* **102**, 054418 (2020).
- [41] M. Feyngenson, D. Novoselov, S. Pascarelli, R. Chernikov, O. Zaharko, F. Porcher, D. Karpinsky, A. Nikitin, D. Prabhakaran, A. Sazonov, and V. Sikolenko, Manifold of spin states and dynamical temperature effects in LaCoO_3 : Experimental and theoretical insights, *Phys. Rev. B* **100**, 054306 (2019).
- [42] A. S. Panfilov, G. E. Grechnev, I. P. Zhuravleva, A. A. Lyogenkaya, V. A. Pashchenko, B. N. Savenko, D. Novoselov, D. Prabhakaran, and I. O. Troyanchuk, Pressure effect on magnetic susceptibility of LaCoO_3 , *Low Temp. Phys.* **44**, 328 (2018).
- [43] E. Şaşıoğlu, C. Friedrich, and S. Blügel, Effective Coulomb interaction in transition metals from constrained random-phase approximation, *Phys. Rev. B* **83**, 121101(R) (2011).